Hindawi
International Transactions on Electrical Energy Systems
Volume 2024, Article ID 1335666, 21 pages
https://doi.org/10.1155/2024/1335666

Research Article

Feature Extraction and Classification of Power Quality Disturbances Using Optimized Tunable-*Q* Wavelet Transform and Incremental Support Vector Machine

Indu Sekhar Samanta,[1] **Pravat Kumar Rout**,[2] **Kunjabihari Swain**,[3] **Satyasis Mishra**,[4] **and Murthy Cherukuri**[3]

[1]*Department of Computer Science and Engineering, Siksha 'O' Anusandhan University, Bhubaneswar, India*
[2]*Department of Electrical and Electronics Engineering, Siksha 'O' Anusandhan University, Bhubaneswar, India*
[3]*Department of Electrical and Electronics Engineering, NIST University, Berhampur, Odisha, India*
[4]*Department of Electronics and Communication Engineering, Centurion University of Technology and Management, Bhubaneswar, India*

Correspondence should be addressed to Murthy Cherukuri; chmurthy@nist.edu

Received 12 July 2023; Revised 22 March 2024; Accepted 4 April 2024; Published 29 April 2024

Academic Editor: Hamed Jafari Kaleybar

The widespread integration of renewable energy sources (RESs) into power systems using power electronics-based interface devices has led to a substantial rise in power quality (PQ) issues. There is an immediate requirement for effective monitoring, detection, and classification of power quality disturbances (PQDs) that is needed to take remedial measures and design planning of the system architecture. This study presents a hybrid approach with an objective for the feature extraction and classification of PQDs. The proposed hybrid approach is comprised of an optimized tunable-*Q* wavelet transform (OTQWT) for the feature extraction and incremental support vector machine (ISVM). A four-stage approach is suggested for the PQ detection and classification in this study. In the first stage, the various data are retrieved both in the form of synthetic data by mathematical formulations and real-time data with prototype design setup. In the second stage, regardless of the specified wavelet function, the PQD signals are decomposed into low-pass and high-pass sub-bands using the tunable-*Q* wavelet transform (TQWT). However, the utilization of default decomposition parameters to address nonstationary PQ signals may lead to information loss and reduced performance of the system. To avoid this limitation, an OTQWT as an enhanced technique to TQWT based on an Adaptive Particle Swarm Optimization (APSO) is suggested. A modified objective function based on the mean square error (MSE) is used to improve the decomposition process. In the third stage, an efficient classifier is suggested based on the ISVM. Lastly, to test and evaluate the performance of the proposed approach, twelve types of PQDs including noise and multiple occurrences are considered. The comparative analysis with other popular methods reflects the better performance of the proposed approach and justifies its use for PQ detection and classification purposes in real-time conditions.

1. Introduction

In recent years, there has been a notable transition from traditional power networks to the adaption of smart-grid and microgrid modernization strategies. This transformation involves the integration of renewable energy sources (RESs) into medium and low-voltage distribution networks particularly [1]. The power electronics-based interfacing devices play a crucial role along with energy storage devices (ESDs) to bring a stable operation. Due to these nonlinear devices, microgrids in the present scenario experience higher levels of harmonics and encounter power quality challenges with the pace of increase in RES integration. As a result, a wide range of disturbances such as voltage and current fluctuations, power factor variations, reactive power demands, transients, swell, sag, harmonics, noise, and notches need to be focused and

remedial measures are to be taken to avoid the negative impact on the system performance [2]. From an operational point of view, PQ degradation is predominantly influenced by various factors including changes in utility load conditions, line switching events, nonlinear capacitive and inductive loads, fault conditions, and grid stability. Furthermore, noise contamination at various levels causes a number of PQ disturbances to be exaggerated and complex in form, which significantly contributes to a general drop in PQ [3]. These disturbances have significant repercussions on system operation, including disruption of digital equipment, unexpected trips of circuit breakers and protection relays, and potential damage to sensitive devices such as microprocessor-based gadgets and computers [4, 5]. The first step towards considering these issues in real-time conditions is to monitor, detect, and analyze the PQDs and that helps further steps at the design and implementation level to provide the remedial measures for the low PQ in the system. To effectively address PQ issues, it is crucial to diagnose them following the IEEE-1159 standards [6]. Looking at the criticality of detecting and classifying PQ disturbances in a smart grid, a hybrid approach that prioritizes monitoring and utilizes appropriate diagnostic techniques is necessary. This critical problem is considered as the primary objective and a necessity for a better approach to diagnosing PQDs is the major motivation for this study.

Fast Fourier Transform (FFT) and its variants such as the Discrete Fourier Transform (DFT) and the Short Time Fourier Transform (STFT) are initially popular due to their useful time and frequency analysis properties and simplicity of implementation [5, 7]. Although DFT excels at detecting long-term trends in PQD signals, due to the nonstationary characteristics of power signals, it is unable to identify sudden changes in PQ occurrences [8]. Apart from that due to aliasing effects, picket fencing, and leaking, FFT is unable to accurately determine amplitude, frequencies, and phases in many conditions. The fundamental limitation of the STFT technique that prevents it from being widely used in the investigation of PQ events is its limited resolution in time and frequency [9]. Because of the inherent higher signal-to-noise ratio and higher resolution in the time-frequency domain, the Gabor–Wigner Transform (GT) was a viable alternate option for the PQ analysis. However, the major limitations of the GT like its complex calculation technique and limited high-frequency applications restrict its use in the PQD analysis. With advantages including efficient phase correction, a tunable window size, and a more complete time and frequency representation of signals, the S-transform, a combination of the wavelet transform (WT) and STFT, has found widespread use in PQ analysis in the past two decades of research [10, 11]. Due to drawbacks such as the centre frequency dependence of the frequency window, the constant width of the Gaussian window, and the increased processing time, it fails to result in better performance for PQ analysis [3]. Hilbert–Huang Transform (HHT) is a two-step method that utilizes Empirical Mode Decomposition (EMD) and Hilbert transform (HT) to instantly recover required frequency and amplitude information [12]. HHT's primary drawback is its limited usefulness in a wide variety of contexts [4]. The PQ signals are broken down into individual band-limited intrinsic mode functions (BLIMFs) using variational mode decomposition (VMD) [13]. VMD is superior to EMD in its ability to continually and adaptively ascertain frequency bands and estimate related modes. However, the VMD's principal restrictions are the signal onset and boundary effects. VMD is challenging to apply due to the spectral bands of the modes fluctuation due to the nonstationary nature of PQ occurrences [5]. Another promising method based on Mathematical Morphology (MM) is employed in many detection-based situations [14] because it requires fewer processing tasks and makes use of a simple set and arithmetic theory. However, the MM technique becomes less effective, in particular, with large datasets [5]. All the methods have their pros to perform better for PQ detection and cons to improve for better performance. Even though extensive research has been done, the major research gap is to provide a better approach for feature extraction through signal transformation to analyze the nonstationary PQ power signals.

The electrical power industry has recently shown a growing interest in classifiers based on artificial intelligence [4, 5]. Neural network- (NN-) based classifiers have significant mathematical flexibility and a high percentage of classification accuracy. However, they are less effective due to the need for extensive training with large datasets in noisy real-time environments and complex signal analysis conditions [15–18]. In addition to that the major limitation of NN is its slow convergence speed and its dependency on the underlying system design and parameters. Using rule-based and membership-degree techniques, Fuzzy Logic- (FL-) based classifiers are modelled and able to classify accurately even with overlapping and uncertain signal features [19]. However, the major shortcoming of FL is its need to change the existing topology and system parameters in the case of different sets of datasets for PQ analysis. In addition to the aforementioned techniques, digital filtering and MM, rule-based decision trees, and expert systems are other prominent techniques used as classifiers for PQDs [15, 20–25]. It is an open area of research to date to provide a better classifier for the PQ analysis having robust and consistent performance, reduced computational burden, noise tolerance, and high accuracy.

A four-stage approach is followed in this study as shown in Figure 1. In the first stage known as the data acquisition stage, the nonstationary power signals under various PQ disturbances are recorded in both synthetic data form from mathematical modelling and experimental data form from the prototype model. Based on the data taken from various PQDs, a signal processing technique is applied to compute the most dominant and sensitive features characterizing the PQ signals in the second stage known as the feature extraction stage. In this study, the OTQWT technique is suggested. In stage 3, known as the classification stage, a classifier as a pattern recognition technique is used to accurately classify and detect the PQ signal. In this study, ISVM is suggested. In stage 4, decision stage, the hybrid approach comprised of OTQWT and ISVM is suggested to detect the types of disturbances.

In this study, the key contributions to the identification of PQDs are as follows:

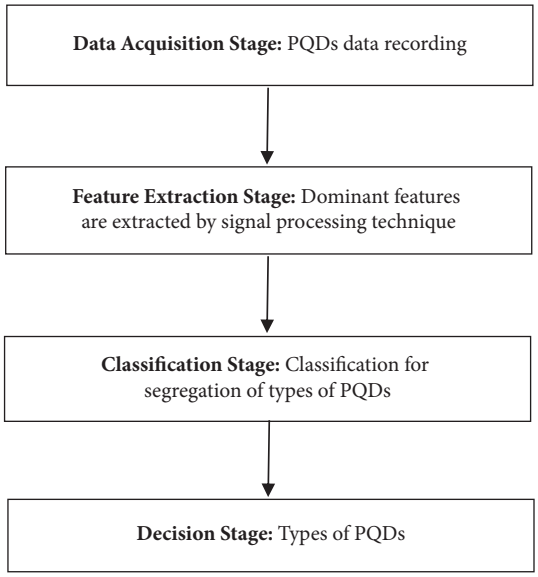

Figure 1: Multistage approach for PQ detection and classification.

(i) The study presents a feature extraction methodology for PQDs based on OTQWT. The OTQWT enables the extraction of five informative characteristics in terms of dominating features that facilitate precise classification. Furthermore, the study addresses the limitations of WT and Empirical Wavelet Transform (EWT) techniques in handling nonstationary PQD signals by successfully implementing OTQWT.

(ii) The classification of PQDs is performed using the ISVM technique. Compared to traditional SVM and Least Square Support Vector Machine (LSSVM) classifiers, ISVM demonstrates superior accuracy in classifying PQDs. This PQ event recognition method looks at all possible single and complex power quality events, with and without noisy conditions.

(iii) The optimized TQWT is suggested based on the APSO titled OTQWT avoiding the randomly selected system parameters.

(iv) The efficacy and validity of the OTQWT-ISVM hybrid method are substantiated and verified through extensive simulation results and testing using hardware prototypes.

The rest of the paper is organized as follows. In Section 2, stage 2 of the proposed approach, feature extraction through the OTQWT is presented in detail. In Section 3, stage 3 of the approach, classification based on the ISVM is detailed. The result analysis based on the synthetic data is presented in Section 4. In addition to this, the result analysis by the prototype experimental setup with experimental data is illustrated and analyzed. Finally, the paper concludes with its critical findings as the concluding remarks of the study with the future scope of the work.

2. Feature Extraction by OTQWT

2.1. Basics of WT. The ability of WT to analyze the local discontinuities of the signals can be best used for steady-state analysis and the analysis of signals in various fields having nonstationary characteristics [26]. The PQDs of the power system have nonstationary characteristics; hence, the WT is preferred as a suitable tool for PQD detection. The continuous signal $u(t)$ in the Continuous WT (CWT) form can be mathematically expressed with the wavelet function $\psi_c(t)$ as

$$\mathrm{CWT}(a,b) = \frac{1}{\sqrt{\mathrm{a}}}\int_{-\infty}^{\infty} u(t)\psi_c\left(\frac{t-b}{a}\right)dt, \quad a,b \epsilon R, a \neq 0. \tag{1}$$

In (1), the scale and translation parameters are represented by the constants a and b, respectively. The scale parameter a provides the oscillatory frequency and wavelet length. The shifting position is well represented by b, the translation parameter. Each scale has a series of wavelet coefficients, which are the output and represent the comprehensive PQ signal [27]. The superfluous information in practical applications of CWT makes it unsuitable for signal analysis. The Discrete WT (DWT) is found more appropriate for analysis of the PQDs and can be expressed as

$$\mathrm{DWT}(m,n) = \frac{1}{\sqrt{a_0^m}}\sum_k u(k)\psi\left(\frac{n - kb_0a_0^m}{a_0^m}\right), \tag{2}$$

where a_0^m and $kb_0a_0^m$ represent the scaling parameter and the translation parameter, respectively. The discrete point sequences represented by $u(k)$ are considered the discrete form of the continuous-time signal $u(t)$. Depending on the type of data used in WT applications, selecting the mother wavelet type has a significant role in analyzing the signal. Among different types of mother wavelets, the Daubechies mother wavelet at scale 4 (db4) has a significant role in feature extraction and is widely used for different applications [28].

2.2. Empirical Wavelet Transform. Based on the $s(t)$ signal's maxima, the Empirical Wavelet Transform (EWT) is an adaptive sub-band decomposition method [29]. The range of the frequency considered in EWT is $\omega \epsilon [0, \pi]$, and the spectrum is symmetric around $\omega = 0$. The range of the existing segment is between $\omega_0 = 0$ and $\omega_n = \pi$, and the segment is denoted as $\Lambda_{tn} = [\omega_{n-1}, \omega_n]$. The empirical wavelets in the bandpass filter on each segment are Λ_{tn}. Signal empirical wavelets' inner products give detailed coefficients, $[D_{tf}^{\varepsilon}(n,t)]$, as follows:

$$D_{tf}^{\varepsilon}(n,t) = \langle s, \psi_{tn}\rangle = \int s(\tau).\overline{\psi_{tn}(\tau - t)}d\tau = \left\{\widehat{s}(\omega).\overline{\widehat{\psi}_{tn}(\omega)}\right\}^{\vee}, \tag{3}$$

where $\widehat{\psi}_{tn}(\omega)$ denotes the empirical wavelet function and is represented as

$$\widehat{\psi}_{tn}(\omega) = \begin{cases} 1, & \text{if } \omega_n + \tau_n \le |\omega| \le \omega_{n+1} - \tau_{n+1}, \\ \cos\left[\frac{\pi}{2}\beta_t\left(\frac{1}{2\tau_{n+1}}\left(|\omega| - \omega_{n+1} + \tau_{n+1}\right)\right)\right], & \text{if } \omega_{n+1} - \tau_{n+1} \le |\omega| \le \omega_{n+1} + \tau_{n+1}, \\ \sin\left[\frac{\pi}{2}\beta_t\left(\frac{1}{2\tau_n}\left(|\omega| - \omega_n + \tau_n\right)\right)\right], & \text{if } \omega_n - \tau_n \le |\omega| \le \omega_n + \tau_n, \\ 0, & \text{Otherwise.} \end{cases} \tag{4}$$

2.3. Optimized Tunable Q Wavelet Transform (OTQWT)

2.3.1. Tunable Q Wavelet Transform (TQWT). TQWT is a recently developed transform designed in such a manner to adjust the Q factor more easily and continuously [30]. The main motivation for developing TQWT is to represent oscillatory signals efficiently. Modifying the Q factor of the wavelet transform to reflect the signal's oscillatory nature allows for a sparse representation of the oscillatory signals. The improved sparsity enhances the performance of the signal processing algorithms based on sparsity in the application fields of signal separation, classification, denoising, and deconvolution. The easily specified input arguments of the TQWT are Q-factor (Q), total oversampling rate (r), and the number of decomposition stages (J) [31]. The oscillations of the wavelet and the frequency response overlapping are managed by the parameters Q and r, respectively. Each frequency response becomes more truncated as Q rises, resulting in an increased number of decomposition levels across the same frequency range. The increase in r for a fixed value of Q results in the overlapping of adjacent frequency responses and demands an increase in levels of decomposition to mask the same frequency range. Using the nonrational transfer function makes this transform suitable for the frequency domain. The low-pass subband signals can be filtered using a two-band filter bank to achieve a multistage decomposition using TQWT. Figure 2 represents the J-level tunable Q wavelet decomposition (TQWD).

A high-pass sub-band (HPS) signal with $\beta_t f_{ts}$ as the sampling frequency and a low-pass sub-band (LPS) signal with $\alpha_t f_{ts}$ as the sampling frequency are generated from the input oscillatory signal $v_t[n]$ with a sampling rate of f_{ts} [30]. α_t and β_t are the scaling parameters. After applying the low-pass filter, $F_{t0}(\omega)$, and the low-pass scaling, LPS α_t, we obtain the low-pass sub-band. High-pass subbands are also realized with high-pass filters, such as $F_{t1}(\omega)$ and HPS β_t. Low-frequency signal components are maintained by LPS α_t, while high-frequency signal components are maintained by HPS β_t [31]. The low-pass and high-pass filters used in TQWT are represented in (5) and (6), respectively

$$F_{t0}(\omega) = \begin{cases} 1, & |\omega| < (1-\beta_t)\pi, \\ \left(\frac{\omega + (\beta_t - 1)\pi}{\alpha_t + \beta_t - 1}\right), & \theta(1-\beta_t)\pi \le |\omega| < \alpha_t\pi, \\ 0, & \alpha_t\pi < |\omega| \le \pi. \end{cases} \tag{5}$$

$$F_{t1}(\omega) = \begin{cases} 0, & |\omega| < (1-\beta_t)\pi, \\ \theta\left(\frac{\alpha_t\pi - \omega}{\alpha_t + \beta_t - 1}\right), & (1-\beta_t)\pi \le |\omega| < \alpha_t\pi, \\ 1, & \alpha_t\pi < |\omega| \le \pi. \end{cases} \tag{6}$$

The frequency response of the two vanishing moments of the Daubechies filter can be represented by (ω), which is the 2π-periodic power complementary function. (ω) can be expressed as [31]

$$\theta(\omega) = 0.5\,(1 + \cos(\omega))\sqrt{2 - \cos(\omega)}. \tag{7}$$

The same filter bank applied for decomposition may be used to reconstruct the initial input signal. The expression of the parameters r and Q in terms of α_t and β_t is as follows:

$$r = \frac{\beta_t}{1 - \alpha_t}, \qquad Q = \frac{f_c}{BW} = \frac{2 - \beta_t}{\beta_t}. \tag{8}$$

After decomposing the input signal into J levels, we get a frequency response in sub-band-J with a centre frequency of f_c and a bandwidth of BW.

2.3.2. Optimized Tunable Q Wavelet Transform (OTQWT). The application of TQWT is found in several signal decompositions for its ability to tune the parameters Q and r following the nonstationary behaviour of the signal. The empirical choice of the fixed decomposition parameters Q, r, and J may result in higher reconstruction error and increase the chances of misclassification and performance degradation. Each highly nonstationary PQD signal may require

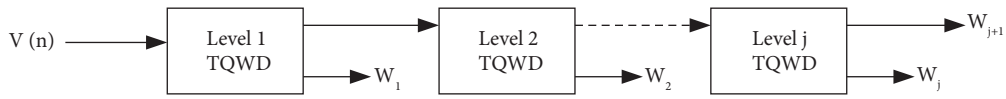

Figure 2: J-level tunable Q wavelet decomposition.

unique decomposition parameters for enhanced approximation and decomposition. The OTQWT is proposed as a solution to the problem of TQWT's decomposition parameters being chosen empirically. Decomposition parameters are selected by the OTQWT in an adaptive fashion that takes into account the specifics of PQD signals. When parameters are chosen correctly, the amount of reconstruction error is minimized, and the optimal number of sub-bands is achieved. For a better collection of information from the extremely oscillatory signals, the value of Q is chosen as ≥ 1. The selection of the value of the redundancy rate $(r) \geq 3$ results in better time-domain localization. To collect detailed information about the signal, it is required to select an optimized value of Q and r. Equations (9) and (10) represent the frequency response of LPS $(W_{t0}^{J}(\omega))$ and $(W_{t1}^{J}(\omega))$, respectively.

$$W_{t0}^{J}(\omega) = \begin{cases} \Pi_{j=0}^{J-1} W_{t0}\left(\dfrac{\omega}{\alpha_t^j}\right), & |\omega| \leq \alpha_t^j \pi, \\ 0, & \alpha_t^j \pi < |\omega| \leq \pi. \end{cases} \tag{9}$$

$$W_{t1}^{J}(\omega) = \begin{cases} W_{t1}\left(\dfrac{\omega}{\alpha_t^{J-1}}\right)\Pi_{j=0}^{J-2} W_{t0}\left(\dfrac{\omega}{\alpha_t^j}\right), & (1-\beta_t)\alpha_t^{j-1}\pi \leq |\omega| \leq \alpha_t^{j-1}\pi, \\ 0, & \omega \epsilon\, [-\pi, \pi]. \end{cases} \tag{10}$$

The LPS and HPS frequency responses are governed by the low-pass scaling parameter α_t and the high-pass scaling parameter β_t. α_t and β_t collect information about the low-frequency and high-frequency components of the signal, respectively. So, the proper selection of α_t and β_t is essential to follow the highly complex behaviour of the PQD signals. Equations (11) and (12) denote the expression of high-pass scaling (β_t) and low-pass scaling (α_t), respectively.

$$\beta_t = \frac{2}{Q+1}, \tag{11}$$

$$\alpha_t = 1 - \frac{\beta_t}{r}. \tag{12}$$

Properly selecting the decomposition level has an important role in restricting the vanishing sub-bands. The number of decomposition levels is kept smaller than the maximum for better performance. The maximum decomposition level $(J_{t\max})$ can be expressed as

$$J_{t\max} = \left| \frac{\log(N/4(Q+1))}{\log(Q+1/Q+1-2/r)} \right|. \tag{13}$$

From equations (11)–(13), it can be observed that the quality factor Q and redundancy rate r have full control over the values of α_t and β_t and the selection of the maximum level of decomposition. The finding of optimum values of Q and r results in obtaining the optimal values of α_t, β_t, and $J_{t\max}$. In this technique, the values of Q and r are selected following the nature of the PQD signals. The PQD signal in its decomposed form can be represented as

$$y_t(t) = \hat{y}_t(t) + e_{td}(t), \tag{14}$$

where $\hat{y}_t(t)$ denotes the approximated signal found by inverse OTQWT and $e_{td}(t)$ denotes the error of decomposition. The inverse OTQWT gives the approximated signal and can be expressed as

$$\hat{y}_t(t) = \sum_{j=1}^{J_{t\max}} V_{tj}, \tag{15}$$

where V_{tj} denotes the j^{th} level sub-band of OTQWT.

Figure 2 reveals that the sub-bands of the TQWT are more dependent on the low and high-pass scaling and the LPS and HPS frequency responses. So, the optimum values of the parameters Q and r ensure an enhanced signal approximation. The manual selection of the parameters Q and r for minimum error $e_{td}(t)$ in the decomposition of the PQD signals is a monotonous task. For a better matching of the approximated signal $\hat{y}_t(t)$ with the original signal $y_t(t)$, the application of optimization techniques is required for the adaptive selection of these parameters. Equation (16) represents the objective function, $x_{te}(t)$, used for optimization.

$$x_{te}(t) = \int_{-\infty}^{+\infty} \left(y_t(t) - \hat{y}_t(t)\right)^2 dt. \tag{16}$$

The search for each optimization algorithm begins with the primary set of values of the solution. This technique uses PSO to minimize the decomposition error. In PSO, the movement of the entire population is towards the fittest individual for the generation of the new population. Equation (17) denotes the updated expression of the PSO.

$$(Q,r)_i = \xi_p\Big(I_p * V_{pi} + C_{p1}\big((Q,r)P_{\text{pbest}} - (Q,r)_i\big) + C_{p2}\big((Q,r)G_{\text{pbest}} - (Q,r)_i\big)\Big),$$
$$(Q,r)_{i+1} = (Q,r)_i + V_{pi}, \tag{17}$$

where $(Q,r)P_{\text{pbest}}$ and $(Q,r)G_{\text{pbest}}$ denote the personal solution and global best solution, respectively; V_{pi} denotes the i^{th} particle velocity and $(Q,r)_i$ denotes i^{th} particle position; C_{p1} and C_{p2} are the personal and social cognitive factors; and ξ_p and I_p represent the constriction factor and inertia, respectively.

After obtaining the optimum values of the parameters Q and r, the maximum number of decomposition levels $J_{t\max}$ is computed according to (13). For each PQD signal, different values of $J_{t\max}$ are computed. To have the same decomposition level for each PQD signal, the optimum decomposition level $J_{t\text{opt}}$ is obtained in terms of $J_{t\max}$, as shown in the following equation:

$$J_{t\text{opt}} = \frac{1}{N}\sum_{n=1}^{N} J_{t\max}^{n}, \tag{18}$$

where N denotes the number of PQD signals.

The proposed OTQWT algorithm is as follows (Algorithm 1).

The major limitations of WT are shift sensitivity, poor directionality, lack of phase information, redundancy, and impracticality. The EWT, however, addresses some of the limitations of WT, but it has its limitations of slow running and causes puzzling empirical modes due to frequency domain division. OTQWT addresses the above limitations of WT and EWT and gives better performance for feature extraction than WT and EWT.

2.4. PQD Generation and Signal Transform. Twelve distinct single-type and complex hybrid PQD signals are used to evaluate the suggested method. Following IEEE-1159 [6], single-type and complex hybrid synthetic PQDs are created. The windowed signal for this PQDs investigation was sampled at 3.2 kHz in a 50 Hz system. All PQD signals are 12 cycles in length.

There are 12 distinct PQD signals taken into account here. Sag, swell, momentary interruption, harmonics, spike, notch, impulsive transient, flicker with sag, flicker with swell, sag with harmonics, swell with transient, and flicker with harmonics are represented by PCL1, PCL2, PCL3, PCL4, PCL5, PCL6, PCL7, PCL8, PCL9, PCL10, PCL11, and PCL12, respectively. The effectiveness of the proposed method is evaluated by using real-time experimental signals and combining them with noise signals. In Section 4, we provide a comprehensive breakdown of how to generate various PQ occurrences through both simulation and hardware prototyping.

The transform techniques, i.e., WT, EWT, and OTQWT, are applied to different PQD signals; their results are illustrated in Figures 3–8. Figure 3 demonstrates the WT application on PQD signals like Voltage Sag, Voltage Interruption, Harmonics, and Swell with Harmonics. This figure shows the pictorial form of the above PQD signals and their WT coefficients at 10, 30, and 50 scales. Figure 4 demonstrates the EWT application on PQD signals like Voltage Sag, Voltage Interruption, Harmonics, and Swell with Harmonics. This figure shows the pictorial form of the above PQD signals and Multiresolution Analysis (MRA) at levels 1, 2, 3, and 4. The OTQWT of the harmonics signal is shown in Figure 5 as follows: (a) test signal, reconstructed signal (basic component), an error signal, (b) wavelet sub-bands, (c) frequency response, and (d) wavelet and low-pass scaling function at level 10. The OTQWT of the Sag signal is shown in Figure 6 as follows: (a) test signal, reconstructed signal (basic component), Error signal, (b) wavelet sub-bands, (c) frequency response, and (d) wavelet and low-pass scaling function at level 10. The OTQWT of the interruption signal is shown in Figure 7: (a) test signal, reconstructed signal (basic component), Error signal, (b) wavelet sub-bands, (c) frequency response, and (d) wavelet and low-pass scaling function at level 10. The OTQWT of the complex hybrid disturbance (Swell with harmonics) signal is shown in Figure 8: (a) test signal, reconstructed signal (basic component), Error signal, (b) wavelet sub-bands, (c) frequency response, and (d) wavelet and low-pass scaling function at level 10.

2.5. Feature Extraction. The relevant and most effective features are extracted from the transformed components of the signals after the WT, EWT, and OTQWT transform of the signals. The following five types of features are found to be most effective for characterizing the PQD signals and are explained below.

(1) **$\mathbf{F_t}$ 1:** The RMS value of the fundamental component of the n^{th} cycle is expressed as

$$X_t1_{rms}(n) = \sqrt{\left(\frac{1}{S_t}\sum_{i=(n-1)S_t+1}^{nS_t} x_t1(i)^2\right)}. \tag{19}$$

The order number of the signal cycles is denoted by n, where $n = 1, 2, \ldots, 10$. S_t denotes the samples present in a cycle; $x_t1(i)$ denotes the fundamental signal after sampling and is obtained by OTQWT; X_t1_{rms} represents the fundamental rms vector calculated as follows:

$$X_t1_{rms} = \left[X_t1_{rms}(1), \ldots X_t1_{rms}(n), \ldots X_t1_{rms}(10)\right]. \tag{20}$$

(2) **$\mathbf{F_t}$2:** It denotes the variations of rms values of the input signal:

(1) Initialize $Q = 1$ and $r = 1$
(2) Get $J_{t\max}$ using equation (13)
(3) Decompose the signal by OTQWT using $Q = 1$, $r = 1$ and $J_{t\max}$
(4) Obtain the approximate signal using inverse OTQWT with $Q = 1$, $r = 1$, and N (number of samples)
(5) Find the mean square error, $x_{te}(t)$ using equation (16)
(6) **While** (min(MSE)) **do**
(7) **If** (MSE = = min) **then**
(8) Optimum Q and r
(9) **Else**
(10) Iterate with different Q and r
(11) **End if**
(12) **End while**
(13) Choose the values of Q_{opt} and r_{opt} for minimum MSE
(14) Find $J_{t\max}$ from Q_{opt} and r_{opt} for each signal
(15) Repeat steps 1–14 for each PQD signal
(16) Find the optimum decomposition level $J_{t\text{opt}}$ from $J_{t\max}$ using equation (18)
(17) Decompose the PQD signal by OTQWT using Q_{opt}, r_{opt} and $J_{t\text{opt}}$

Algorithm 1: Proposed OTQWT algorithm.

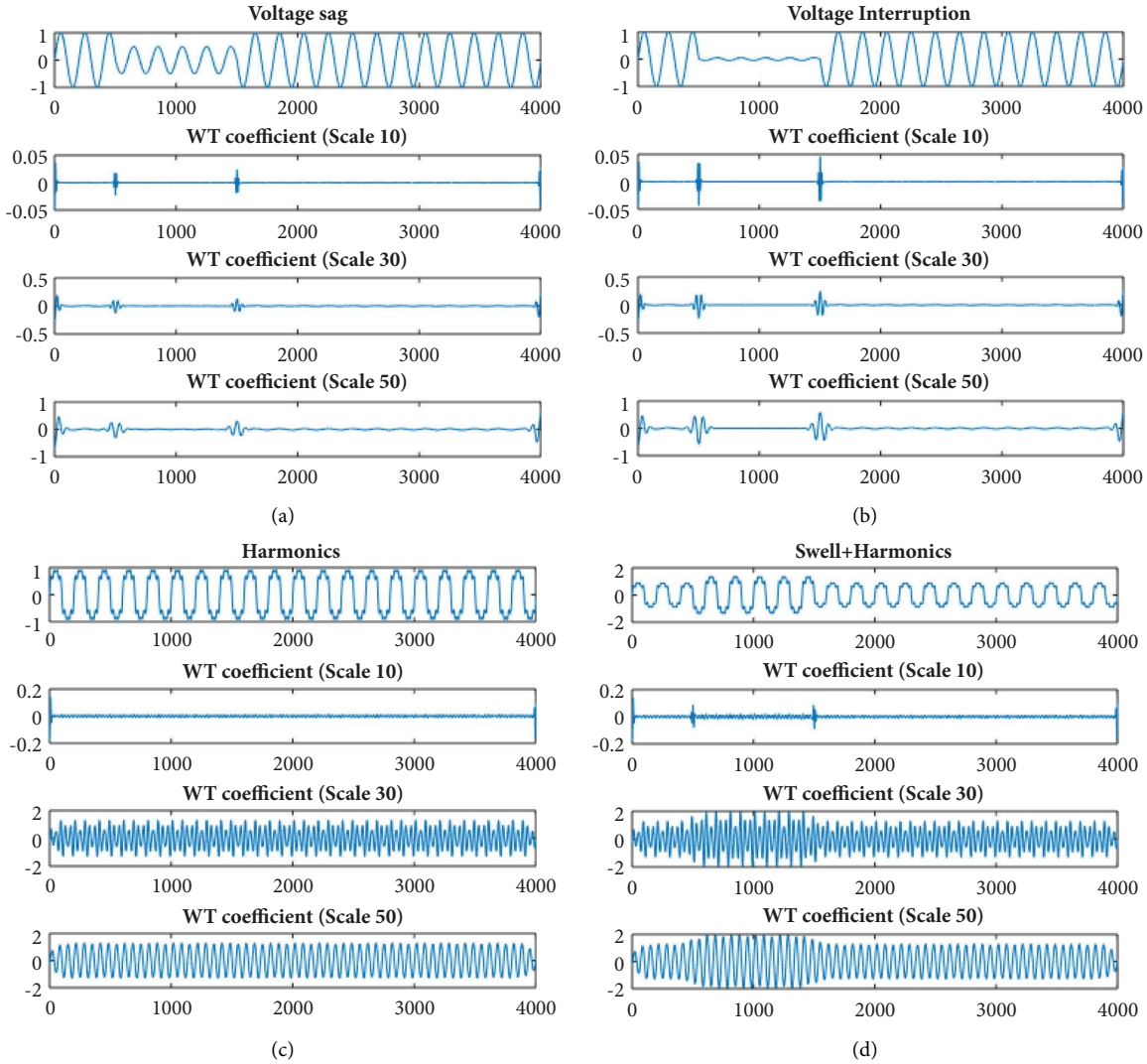

Figure 3: Wavelet transform of (a) voltage sag, (b) interruption, (c) harmonics, and (d) swell with harmonics.

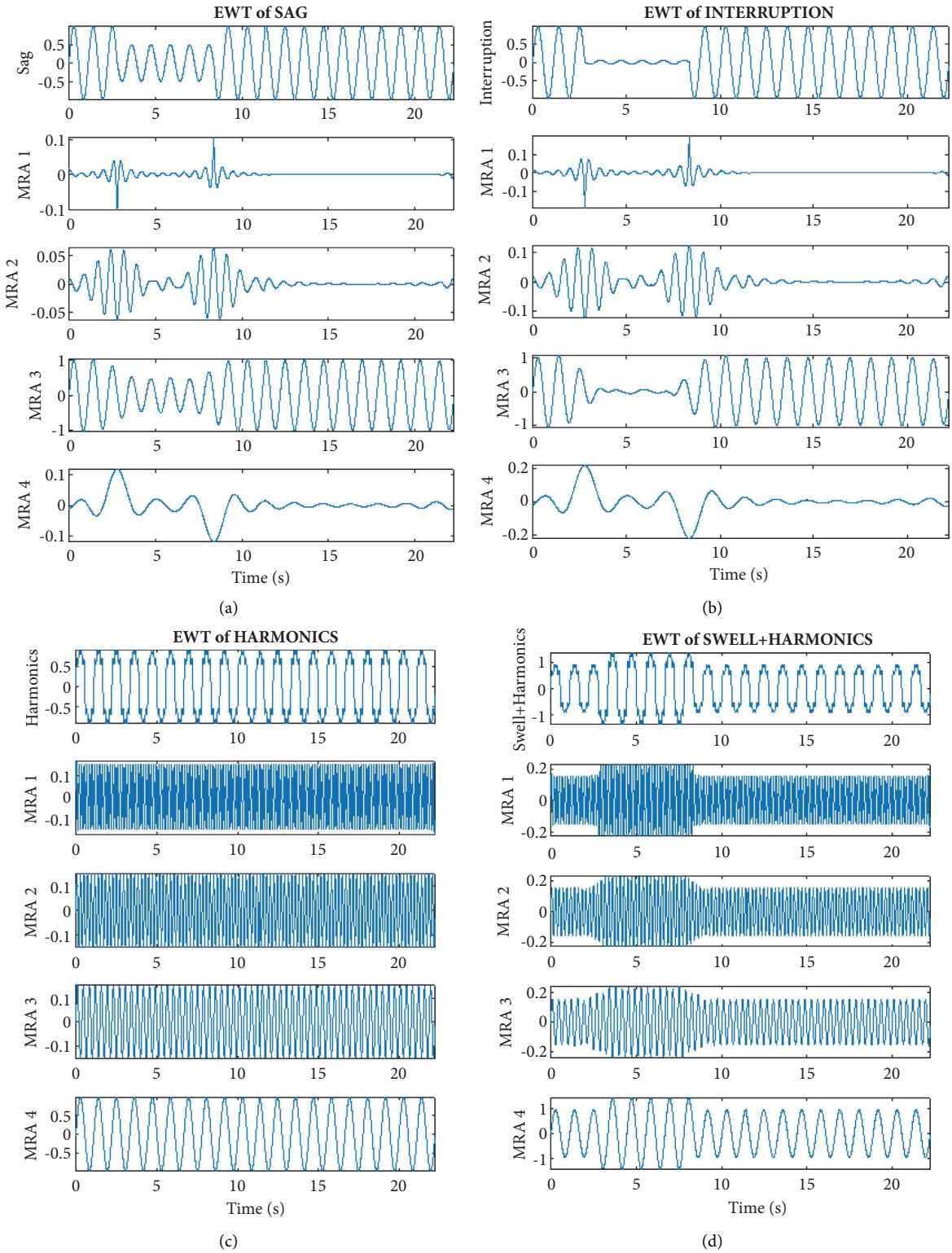

FIGURE 4: Empirical wavelet transform: (a) voltage sag, (b) interruption, (c) harmonics, and (d) swell with harmonics.

$$SV_t(n) = X_{trms}(n) - X_{trms}(n-1), \tag{21}$$

where $X_{trms}(n)$ denotes the rms of the n^{th} cycle of the signal. The feature is expressed as

$$F_t 2 = SV_{t\max} = \max(|SV_t|). \tag{22}$$

(3) **F_t3:** The rms value oscillation of the PQ signal is found as follows:

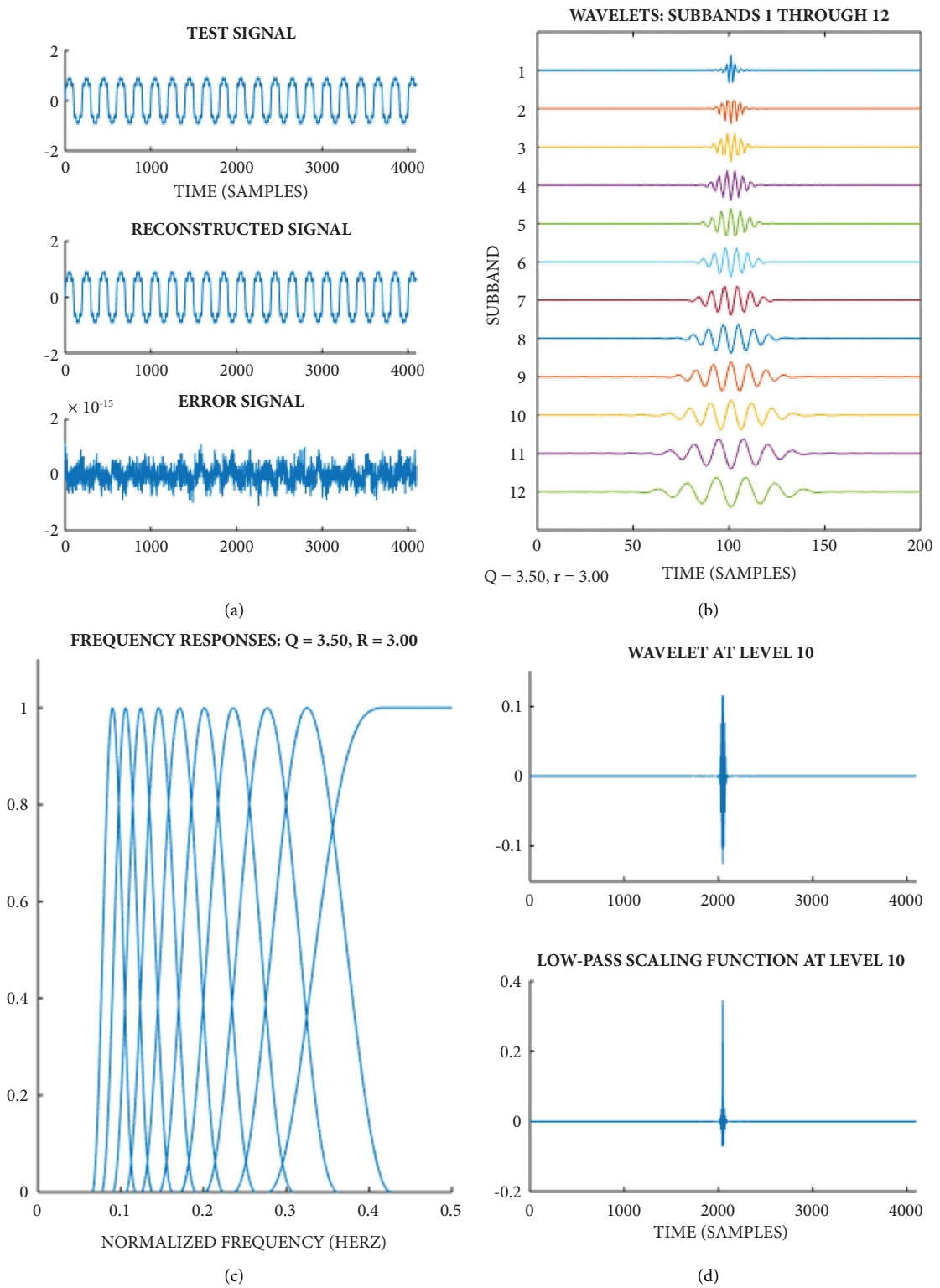

FIGURE 5: OTQWT of harmonics signal: (a) test signal, reconstructed signal (fundamental component), and an error signal, (b) wavelet subbands, (c) frequency response, and (d) wavelet and low-pass scaling function at level 10.

$$\mathbf{SO_t} = \mathbf{X_{trms}} - \text{mean}\left(\mathbf{X_{trms}}\right). \tag{23}$$

The feature $\mathbf{F_t3 = NZ}$ denotes the number of zero crossings found in the oscillation vector, $\mathbf{SO_t}$. $\mathbf{F_t3 \geq 3}$, denotes the low-frequency form of the interharmonics or flicker.

(4) $\mathbf{F_t4}$: This feature helps to recognize the presence of harmonics and transients. The rms value of the high-

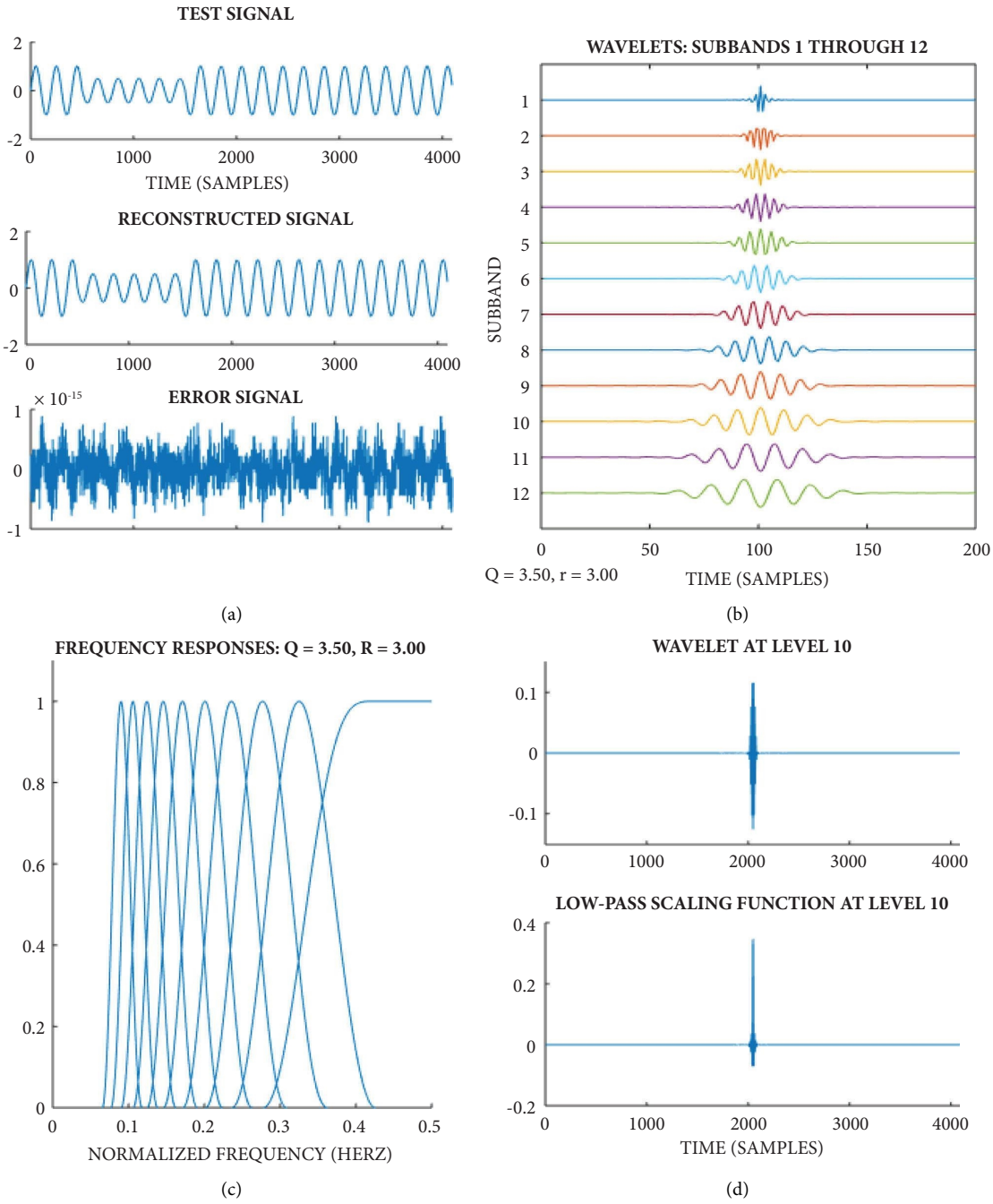

Figure 6: OTQWT of sag signal: (a) test signal, reconstructed signal (fundamental component), and an error signal, (b) wavelet sub-bands, (c) frequency response, and (d) wavelet and low-pass scaling function at level 10.

frequency harmonics of the n^{th} cycle can be computed as

$$X_{t\text{Hrms}}(n) = \sqrt{\left(\frac{1}{S_t}\sum_{i=(n-1)S_t+1}^{nS_t} x_{th}(i)^2\right)}, \tag{24}$$

where $x_{th}(i)$ denotes the harmonic signal having frequency components 300 Hz and above. The per cycle high-frequency harmonic distortion is computed as

$$\text{HHD}_t(n) = \frac{X_{t\text{Hrms}}(n)}{X_t 1_{\text{rms}}(n)}. \tag{25}$$

Thus, the fourth feature refers to the mean distortion values of these high-frequency harmonics.

$$F_t 4 = \text{HHD}_{\text{tm}} = \text{mean}(\text{HHD}_t). \tag{26}$$

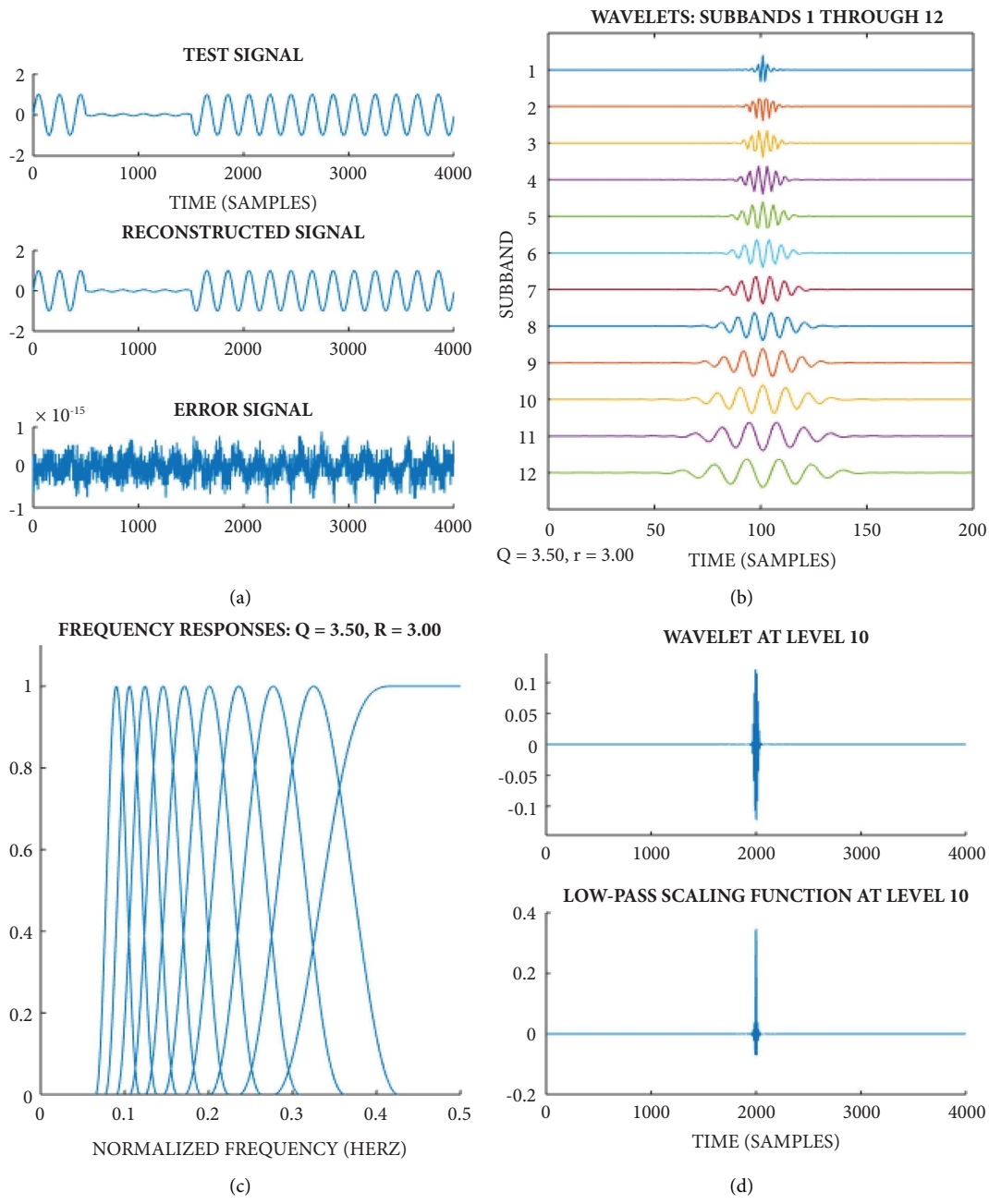

FIGURE 7: OTQWT of interruption signal: (a) test signal, reconstructed signal (fundamental component), and an error signal, (b) wavelet sub-bands, (c) frequency response, and (d) wavelet and low-pass scaling function at level 10.

(5) **F_t5:** The fifth feature is the standard deviation of the fundamental rms vector, as given below:

$$F_t5 = \mathrm{SD} = \mathrm{std}\left(X_t1_{\mathrm{rms}}\right). \tag{27}$$

3. ISVM Classification Method

3.1. Support Vector Machine (SVM). One of the supervised classification techniques widely used in machine learning is the support vector machine [32]. In order to create a model, SVM has been trained using the training data $\{t_{r1}, \ldots, t_{rn}\}$ and class labels $\{l_1, \ldots, l_n\}$, where t_{ri} belongs to R^n and l_i belongs to $\{-1, 1\}$. The class of the new testing samples can be predicted using this model. Creating a hyperplane to maintain a maximum margin between adjacent classes is the main idea behind SVM. The hyperplane reduces the generalization error while classifying a new data point. For a two-class problem, a straight line is used for the separation, but in multidimensional space, a hyperplane separates different classes [33]. In clustering data points, where the linear separation does not work, the data points are mapped into higher dimensional feature space to make the linear separation possible. The same hyperplane is linear in feature space but is nonlinear in the respective input space.

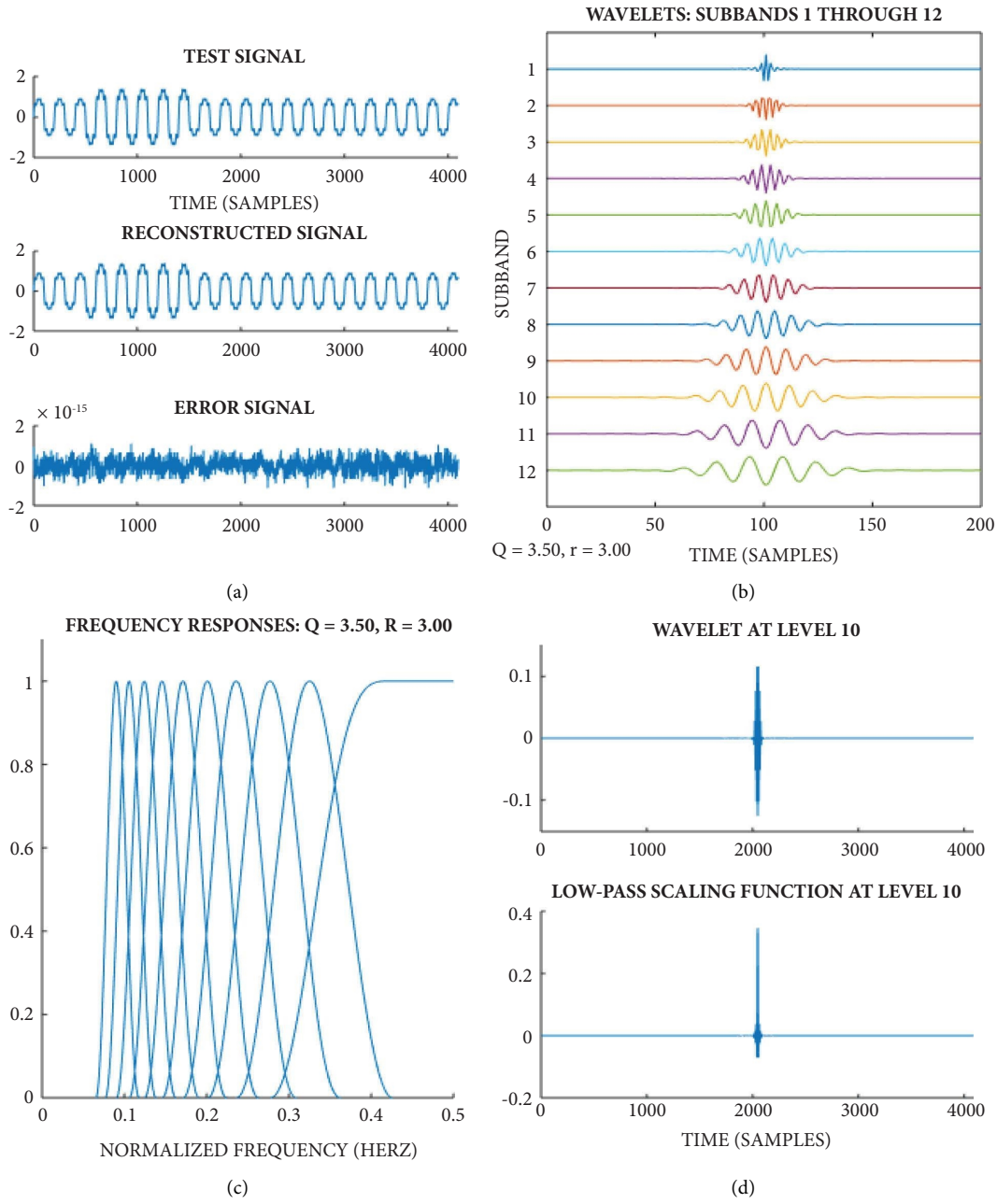

Figure 8: OTQWT of swell with harmonics signal: (a) test signal, reconstructed signal (fundamental component), and error signal, (b) wavelet sub-bands, (c) frequency response, and (d) wavelet and low-pass scaling function at level 10.

The objective of SVM is to create a hyperplane in a two-case scenario with two variables, s_1 and s_2, and can be expressed in the form $w_1 s_1 + w_2 s_2 - b = 0$ with $w_1 s_1 + w_2 s_2 - b \geq 1$ and $w_1 s_1 + w_2 s_2 - b \geq -1$ as the bounding planes. The scalar b denotes the bias term. The appropriate $w_{i,s}$ and b are found during the training stage of SVM [34]. The decision boundary is found as $w^T t_r - b = 0$, once the values of $w_{i,s}$ and b are obtained. Here w denotes a vector. On the arrival of new data points, the label is found with the help of the function as follows:

$$f(t_r) = \text{sign}\left(w^T t_r - b\right). \tag{28}$$

3.2. Least Square Support Vector Machine (LSSVM). The LSSVM is the modified form of SVM proposed by Suykens and Vandewalle [35]. The inequality constraints of SVM are replaced by equality in LSSVM. The training speed of SVM is increased by implementing the gradient function as an empirical risk function and using equality constraints in

LSSVM. The squared error and the loss function of the training set are summed as LSSVM.

Considering $\{x_{li}, y_{li}\}_{i=1}^{N}$ as a training set with N number of items, the formulation of the optimization problem for the prediction of functions may be formulated as

$$\min_{w_l, b_l, e_l} j_l(w_l, e_l) = \frac{1}{2} w_l^T w_l + \gamma_l \frac{1}{2} \sum_{i=1}^{N} e_{\mathrm{li}}^2, \tag{29}$$

with the equality constraints

$$y_{li} = W_l^T \varphi_l(x_{li}) + b_l + e_{li}, \quad i = 1, 2, \ldots, N, \tag{30}$$

where φ_l: $R^n \longrightarrow R^{nh}$ denotes a function that maps the input data into a higher dimensional feature space, W_l denotes the weight vector of the initial weight area, e_{li} denotes error parameter, b_l denotes the bias term, $x_{li} \in R^n$ denotes the input data, and $y_{li} \in R^n$ denotes the output data.

The Lagrangian can be introduced as

$$L(w_l, b_l, e_l, \alpha_l) = J_l(w_l, e_l) - \sum_{i=1}^{N} \alpha_{li} \left\{ W_l^T \varphi_l(i) + b_l + e_l - y_{li} \right\}, \tag{31}$$

where Lagrangian $\alpha_l = (\alpha_{l1}, \alpha_{l2}, \ldots, \alpha_{\mathrm{lN}})$ is the factor vector.

The optimization conditions are as follows:

$$\begin{aligned} &\frac{\partial L}{\partial W_l} = 0 \longrightarrow W_l = \sum_{i=1}^{N} \alpha_{li} \phi(x_{li}), \\ &\frac{\partial L}{\partial b_l} = 0 \longrightarrow b_l = \sum_{i=1}^{N} \alpha_{li} = 0, \\ &\frac{\partial L}{\partial e_l} = 0 \longrightarrow e_l = \frac{1}{C} \alpha_{li}, \quad i = 1, 2, \ldots, N, \\ &\frac{\partial L}{\partial \alpha_{li}} = 0 \longrightarrow y_{li} = W_l^T \varphi_l(x_{li}) + b_l + e_{li}, \quad i = 1, 2, \ldots, N. \end{aligned} \tag{32}$$

The prediction of the LSSVM function is as follows:

$$y_l(x_l) = \sum_{i=1}^{N} \alpha_i K(x_l, x_{li}) + b_l. \tag{33}$$

3.3. Incremental Support Vector Machine (ISVM). The support vector machine (SVM) is a widely used, sparse, and robust binary classification model. The approach of the SVM is to maximize the classification interval in binary classification by optimizing the hyperplane in the feature space [32–34]. The kernel function enables SVM to solve nonlinear and high-dimensional classification problems. This approach makes the problem linearly separable by mapping the low-dimensional space samples to high-dimensional space samples. An incremental support vector machine (ISVM) is proposed to train data online compared to the batch import of training data, as in the case of SVM. ISVM accommodates new samples by gradually adapting the parameters instead of repeatedly training all samples [35–37]. The brief introduction of ISVM is as follows:

(i) For the generation of an ISVM, it is necessary to create a discriminant function $f_t(x) = \omega_t.\phi_t(x) + b_t$ learned from the samples $\{(x_{ti}, y_{ti}) \in \mathbb{R}^m \times \{-1, 1\}, \forall i \in \{1, \ldots, N\}\}$. That implies solving a problem of quadratic programming:

$$\begin{cases} \min\limits_{\omega_t, b_t} \ 1/2 \parallel \omega_t \parallel^2 + C_t. \sum\limits_{i=1}^{N} \varepsilon_{ti}, \\ s.t.\ y_{ti}(\omega_t.x_{ti} + b_t) \geq 1 - \varepsilon_{ti}, \quad i \in \{1, \ldots, N\}. \end{cases} \tag{34}$$

The first term denotes the maximized interval distance, and the second represents the regularization term. C_t denotes the penalty parameter and ε_{ti} denotes the slack variable used for building a soft margin.

(ii) The quadratic program in its dual form is used to deal with the nonlinear issues and is expressed as

$$\min_{0 \leq \alpha_{ti} \leq C_t} : \mathrm{L} = \frac{1}{2} \sum_{i,j} \alpha_{ti} Q_{tij} \alpha_{tj} - \sum_{i} \alpha_{ti} + b_t \sum_{i} y_{ti} \alpha_{ti}, \tag{35}$$

where $Q_{tij} = y_{ti} y_{tj} K(x_{ti}, x_{tj})$, $K(x_{ti}, x_{tj}) = \varphi_t(x_{ti}).\varphi_t(x_{tj})$ and K denotes the kernel function, which simplifies the calculation and does the mapping of vectors to a high-dimensional feature space.

(iii) The discriminant function of the dual form SVM is expressed as

$$f_t(x) = \sum_{j} \alpha_{tj} y_{tj} K\left(x_{tj}, x\right) + b_t. \tag{36}$$

(iv) The Karush–Kuhn–Tucker (KKT) cases describe the solution of dual parameters $\{\alpha_t, b_t\}$ by the first-order conditions on L:

$$\begin{aligned} &G_{ti} = \frac{\partial L}{\partial \alpha_{ti}} = \sum_{j} Q_{tij} \alpha_{ti} + y_{ti} b_t - 1 \begin{cases} >0, & \alpha_{ti} = 0, \\ =0, & 0 \leq \alpha_{ti} \leq C_t, \\ <0, & \alpha_{ti} = C_t, \end{cases} \\ &\frac{\partial L}{\partial b_t} = \sum_{j} y_{tj} \alpha_{tj} = 0. \end{aligned} \tag{37}$$

(v) The training samples are categorized into three cases according to the KKT conditions: the set of margin support vectors (S_t) with $G_{ti} = 0$, the set of error support vectors (E_t) with $G_{ti} \leq 0$, and the set of the remaining vectors (R_t) with $G_{ti} > 0$.

(vi) In the incremental learning process, the coefficients of the margin vectors change simultaneously as soon as the new samples are introduced continuously to satisfy the KKT conditions for the already trained samples. The KKT conditions for a new sample taken as a candidate support vector may be differentially represented as

$$\Delta G_{ti} = Q_{tim}\Delta\alpha_{tm} + \sum_{j\in S_t} Q_{tij}\Delta\alpha_{tj} + y_{ti}\Delta b_t, \quad \forall i \in D \cup \{m\},$$
$$0 = y_{tm}\Delta\alpha_{tm} + \sum_{j\in S_t} y_{ti}\Delta\alpha_{tj}. \tag{38}$$

The changes in coefficients must satisfy the following conditions as $G_{ti} = 0$ for the set of margin vector $S_t = \{S_{t1}, \ldots, S_{tls}\}$. The condition is as follows:

$$\mathcal{Q}_t \cdot \begin{bmatrix} \Delta b_t \\ \Delta\alpha_{tS_{t1}} \\ \vdots \\ \Delta\alpha_{tS_{tls}} \end{bmatrix} = -\begin{bmatrix} y_{tm} \\ Q_{tS_{t1m}} \\ \vdots \\ Q_{tS_{t1m}} \end{bmatrix}\Delta\alpha_{tm}, \tag{39}$$

where $\mathcal{Q}_t$ denotes a symmetric nonpositive definite Jacobian matrix:

$$\mathcal{Q}_t = \begin{bmatrix} 0 & y_{tS_{t1}} & \cdots & y_{tS_{tls}} \\ y_{tS_{t1}} & Q_{tS_{t1}S_{t1}} & & Q_{tS_{t1}S_{tls}} \\ & \vdots & \ddots & \vdots \\ y_{tS_{tls}} & Q_{tS_{tls}S_{t1}} & \cdots & Q_{tS_{tls}S_{tls}} \end{bmatrix}. \tag{40}$$

Then it may be found as

$$\Delta b_t = \beta_t\Delta\alpha_{tm},$$
$$\Delta\alpha_{tj} = \beta_{tj}\Delta\alpha_{tm}, \quad \forall j \in D, \tag{41}$$

with coefficient sensitivities as follows:

$$\begin{bmatrix} \beta_t \\ \beta_{tS_{t1}} \\ \vdots \\ \beta_{tS_{tls}} \end{bmatrix} = -\mathcal{R}_t \cdot \begin{bmatrix} y_{tm} \\ Q_{tS_{t1m}} \\ \vdots \\ Q_{tS_{tlsm}} \end{bmatrix}, \tag{42}$$

where $\mathcal{R}_t = \mathcal{Q}_t^{-1}$ and $\beta_{tj} = 0, \forall j \in$ outside S_t. Now, the KKT conditions in (37) become

$$\Delta G_{ti} = \gamma_{ti}\Delta\alpha_{tm}, \quad \forall i \in D \cup \{m\},$$
$$\gamma_{ti} = Q_{tim} + \sum_{j\in S_t} Q_{tij}\beta_{tj} + y_{ti}\beta_t, \quad \forall\, i \notin S_t. \tag{43}$$

(vii) To affix the candidate vector m into the margin vector set S_t, $\mathcal{R}_t$ is extended as

$$\mathcal{R}_t \leftarrow \begin{bmatrix} & & 0 \\ & \mathcal{R}_t & \vdots \\ & & 0 \\ 0 & \ldots\ 0 & 0 \end{bmatrix} + \frac{1}{\gamma_m}\begin{bmatrix} \beta_t \\ \beta_{tS_{t1}} \\ \vdots \\ \beta_{tS_{tls}} \\ 1 \end{bmatrix}\begin{bmatrix} \beta_t & \beta_{tS_{t1}} & \cdots & \beta_{tS_{tls}} & 1 \end{bmatrix}. \tag{44}$$

On the contrary, extracting a vector k from S_t, $\mathcal{R}_t$ is reduced as

$$\mathcal{R}_{tij} \longleftarrow \mathcal{R}_{tij} - \mathcal{R}_{tkk}^{-1}\mathcal{R}_{tik}\mathcal{R}_{tkj}, \quad \forall i, j \in S_t \cup \{0\}; i, j \neq k. \tag{45}$$

Therefore, when a new sample m is combined with the training dataset D: $D^{l+1} = D^l \cup \{m\}$, then the solution of the parameters $\{\alpha_t, b_t\}$ is revised corresponding to the candidate x_{tm}, y_{tm}, the recent solution, and the inverse Jacobian matrix $\mathcal{R}_t$.

The summarized incremental procedure is as follows:

(1) Initialize α_{tm} to zero, and calculate G_{tm};

(2) If $G_{tm} > 0$, stop (m does not represent error or margin vector);

(3) If $G_{tm} \leq 0$, do the highest attainable increment α_{tm}, to ensure one of the following situations:

(a) $G_{tm} = 0$: Margin set S_t to be added with m, do the corresponding upgradation of $\mathcal{R}_t$ and stop;

(b) $\alpha_{tm} = C_t$: Error set E_t is to be added with C_t, stop;

(c) Elements belonging to D^l move across S_t, E_t, and $\mathcal{R}_t$: Do the membership upgradation of elements and repeat Step 3. If S_t is changing, then do the upgradation of $\mathcal{R}_t$, subsequently.

The SVM classification method performs poorly for large datasets and noisy conditions. A high training time and no probabilistic-related explanations for classification make SVM a poor performer. On the other hand, LSSVM has a poor performance on chaotic input data samples. It consumes a lot of time and requires a priori knowledge for the parameter-optimized methods. The above limitations of SVM and LSSVM are well addressed in ISVM.

4. Result Analysis and Discussion

4.1. Simulation. Twelve distinct single-type and complex hybrid PQD signals are used to evaluate the suggested method. Following IEEE-1159 [6], single-type and complex

hybrid synthetic PQDs are created. Each of the twelve PQDs has a fundamental frequency of 50 Hz and is sampled at 3.2 kHz. In this analysis, a windowed signal of 12 cycles per PQD is taken into account. There are a total of 1200 samples in the database, and 100 of each PQD are used in the experiment. The effectiveness of the proposed strategy was further tested in an experiment with noise levels of 20, 30, and 50 dB. The database has been split so that 60% of it displays training data and 40% displays testing data. All of the work in this experiment was done in MATLAB R2018. The Lenovo laptop with 4 GB of RAM and a 2.20 GHz processor is used to run the proposed algorithms.

4.2. Hardware Experimental Setup. The hardware prototype consists of (i) 1KΩ, 300 V, 2A resistive load, (ii) nonlinear inductive and capacitive loads, (iii) a DAQ of National Instrument make (USB 6001), (iv) a 230/6 volt single phase transformer, and (v) a computer with LabVIEW and MATLAB software. Different load-switching and fault conditions are maintained to experiment with the generation of different PQD signals. A step down of the voltage at 0–6 volt range has been maintained to get data for the computer using USB 6002 DAQ. The data acquisition is performed using LabVIEW 2018 and the NI-DAQmx 18.0.0 device driver. Information is sent between LabVIEW and MATLAB using the TCP/IP connection. The computerized experimental setup is depicted in Figure 9. A recorded waveform from the load is shown in LabVIEW and MATLAB in Figure 10. Load circumstances of linear and nonlinear loads under varying switching conditions generate distinct PQD signals.

Twelve groups of separate and combined PQD signals have been used to categorize the efficacy of the proposed technique. The fundamental frequency in this implementation is 50 Hz, and the sampling frequency for PQD is 3.2 kHz. All PQD signals are 12 cycles in length. There are a total of 1200 samples in the database, 100 from each PQD. An experiment was also conducted in noise conditions (with noise levels of 20, 30, and 50 dB) to measure the efficiency of the proposed strategy.

As evidenced by four separate classification methods, the superior performance of the proposed OTQWT-ISVM-based PQDs detection and classification method is justified. Different PQD signals are taken into account, and their distinguishing characteristics are retrieved. The retrieved features serve as input data for the ISVM classifier, which determines the precise type of PQD. To evaluate the effectiveness of the suggested method, 1200 datasets are used, 100 from each of the 12 class labels. This work follows the common practice of using 60% of the dataset for training and 40% for testing. Classification results for the OTQWT-ISVM method are shown in Tables 1 through Table 2 for both noise-free and noisy (20, 30, and 50 dB) settings.

In the feature extraction phase, five features are extracted from 12 cycles of windowed PQ disturbance signals. The effectiveness of PQD patterns is evaluated using the classic support vector machine (SVM) and the LSSVM that it inspired. Classification results for simulated MATLAB implementations of SVM and LSSVM hybrids with WT, EWT, and OTQWT approaches are presented in Table 3. Overall classification accuracy can be calculated as the fraction of PQDs that were correctly identified out of all PQDs that were tested. Table 4 displays the noise and noiseless classification accuracy of the WT-ISVM, EWT-ISVM, and OTQWT-ISVM. It can be shown that OTQWT-ISVM performs well in the presence of noise and has a higher classification accuracy rate.

The observation based on the simulation results reveals better detection and classification by OTQWT-ISVM compared to EWT-ISVM and WT-ISVM approaches. Table 5 represents the comparison considering the time for training, time for testing, Root Mean Square Error (RMSE) for training, RMSE for testing, and classification accuracy of OTQWT-ISVM in the noise-less and 20 dB noise addition conditions for different values of Q and r.

Taking into account the expressions listed below [38] might help to evaluate the success of your real-time PQD monitoring system.

$$\begin{aligned}\text{Percentage of Accuracy} &= \frac{\text{Number of recognized PQE signals}}{\text{Total number of tested PQE signals}} \times 100,\\ \text{Percentage of Sensitivity} &= \frac{\text{Number of recognized positive signals}}{\text{Total number of tested positive signals}} \times 100,\\ \text{Percentage of Specificity} &= \frac{\text{Number of recognized negative signals}}{\text{Total number of tested negative signals}} \times 100.\end{aligned} \tag{46}$$

For this analysis, we will refer to the plane voltage sinewave as the ideal positive signal and to all PQ events as the ideal negative signal. Sensitivity is the faultless quality of the hardware system's power supply, whereas specificity denotes its flawed qualities.

To prevent precarious power outages, a real-time PQD monitoring system is mandatory. Table 6 displays the results of testing the proposed OTQWT-ISVM-based real-time hardware PQ event monitoring system with 12 different real-time PQDs and 25 different training chunk sizes.

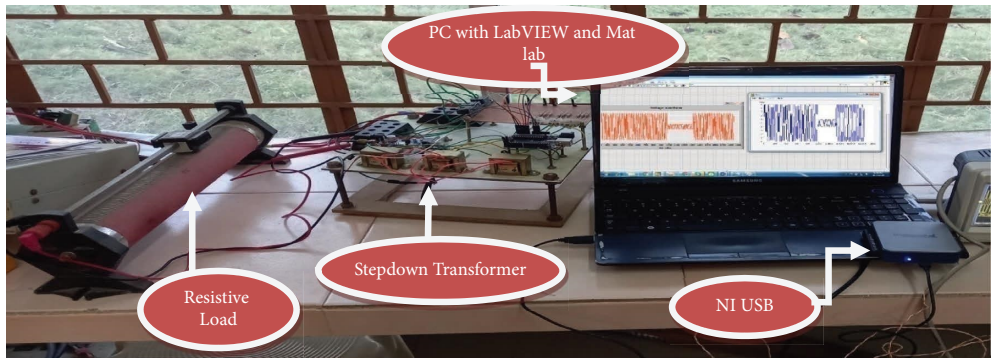

Figure 9: Experimental setup.

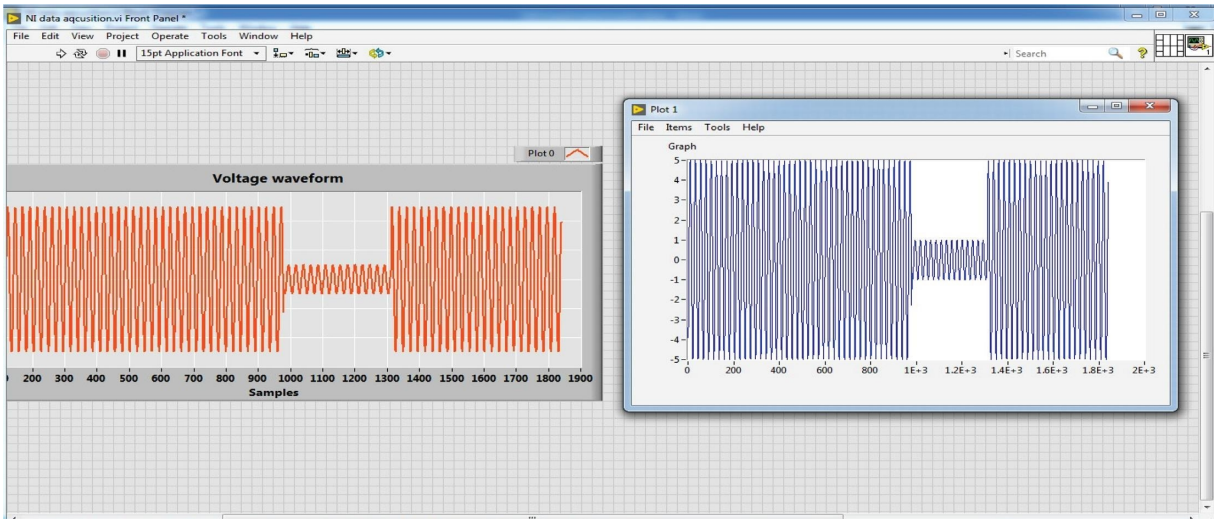

Figure 10: The captured waveform in LabVIEW and MATLAB environments.

Table 1: Classification results of case-1.

Data dimension		Time (in sec.)		Success rate (%)	
Training data	Testing data	Training	Testing	Training	Testing
720	480	0.112	0.0102	99.7	99.64

Table 2: Confusion matrix for case-4.

Events	PCL1	PCL2	PCL3	PCL4	PCL5	PCL6	PCL7	PCL8	PCL9	PCL10	PCL11	PCL12
PCL1	40											
PCL2		40										
PCL3			40									
PCL4				39								
PCL5				1	40							
PCL6						40						
PCL7							40	1			1	
PCL8								39				
PCL9									39			
PCL10									1	40		
PCL11											39	
PCL12												40
Success rate (%)	100	100	100	98.57	100	100	100	98.57	98.57	100	98.57	100

Overall success rate (%): 99.52.

Table 3: Classification with (SVM and LSSVM) and (WT, EWT, and OTQWT).

Methods	Noise-free conditions	Signal-to-noise ratio		
		20 dB	30 dB	50 dB
WT-SVM	88.6	81.9	84.4	86.2
WT-LSSVM	89.3	84	85.9	87.5
EWT-SVM	92.2	87.3	88.8	90.2
EWT-LSSVM	93.7	90	90.4	91.8
OTQWT-SVM	95.6	90.2	91.9	93.9
OTQWT-LSSVM	96.9	91.6	93.3	96

Table 4: Classification accuracy in percentage using WT-ISVM, EWT-ISVM, and OTQWT-ISVM.

Methods	Noise-free conditions	Signal-to-noise ratio		
		20 dB	30 dB	50 dB
WT-ISVM	90.16	87.2	88.5	89.7
EWT-ISVM	94.52	90.4	92.4	92.6
OTQWT-ISVM	99.64	99.52	99.52	99.52

Table 5: Performance comparison of OTQWT-ISVM for different values of Q and r.

Classes	OTQWT-ISVM (with decomposition parameters, $Q = 2.5$ and $r = 3$)						OTQWT-ISVM (with decomposition parameters, $Q = 3.5$ and $r = 3$)					
	Training time (s)	Testing time (s)	Training RMSE	Testing RMSE	Accuracy (%)		Training time (s)	Testing time (s)	Training RMSE	Testing RMSE	Accuracy (%)	
					Noise free-case	20 dB					Noise free-case	20 dB
PCL1	0.0179	0.0130	0.0039	0.0122	100	100	0.0296	0.0197	0.0009	0.0057	100	100
PCL2	0.0158	0.0105	0.0061	0.0227	100	100	0.0275	0.0172	0.0031	0.0161	100	100
PCL3	0.0163	0.0145	0.0038	0.0429	100	98.57	0.0280	0.0212	0.0008	0.0361	100	98.57
PCL4	0.0160	0.0130	0.0041	0.1325	98.57	98.57	0.0277	0.0197	0.0011	0.1151	100	100
PCL5	0.0164	0.0108	0.0118	0.1812	100	100	0.0281	0.0175	0.0088	0.1707	98.57	100
PCL6	0.0177	0.0120	0.0072	0.1387	98.57	98.57	0.0294	0.0187	0.0042	0.1260	100	98.57
PCL7	0.0169	0.0133	0.0105	0.1843	100	100	0.0286	0.0199	0.0075	0.1736	100	100
PCL8	0.0166	0.0117	0.0162	0.3052	98.57	98.57	0.0283	0.0184	0.0132	0.2869	100	98.57
PCL9	0.0164	0.0139	0.0185	0.3015	100	100	0.0281	0.0206	0.0155	0.2887	98.57	100
PCL10	0.0183	0.0145	0.0131	0.0635	100	100	0.0299	0.0212	0.0101	0.0591	100	100
PCL11	0.0179	0.0120	0.0039	0.0118	98.57	98.57	0.0296	0.0187	0.0009	0.0056	98.57	98.57
PCL12	0.0185	0.0145	0.0079	0.1676	98.57	98.57	0.0302	0.0212	0.0049	0.1625	100	100
Mean	0.0170	0.0128	0.0089	0.1303	99.40	99.28	0.0287	0.0195	0.0059	0.1205	99.64	99.52

Table 6: OTQWT-ISVM classification results on real-world test signals.

Classes	PCL1	PCL2	PCL3	PCL4	PCL5	PCL6	PCL7	PCL8	PCL9	PCL10	PCL11	PCL12	Sine wave
PCL1	95	2	0	0	0	1	0	0	1	0	0	0	1
PCL2	1	96	0	0	0	0	0	1	0	0	0	0	2
PCL3	0	0	100	0	0	0	0	0	0	0	0	0	0
PCL4	0	0	0	100	0	0	0	0	0	0	0	0	0
PCL5	0	0	1	0	97	0	1	0	0	1	0	0	0
PCL6	0	0	0	0	0	100	0	0	0	0	0	0	0
PCL7	0	0	0	0	0	0	100	0	0	0	0	0	0
PCL8	0	0	0	0	0	0	0	100	0	0	0	0	0
PCL9	0	0	0	0	0	0	0	0	100	0	0	0	0
PCL10	0	0	0	0	0	0	0	0	0	99	1	0	0
PCL11	0	0	0	0	0	0	0	0	0	0	100	0	0
PCL12	0	0	0	0	0	0	0	0	0	0	0	100	0
Sine wave	0	0	0	0	0	0	0	0	0	0	0	0	100

Accuracy = 99%, sensitivity = 100%, and specificity = 98.91%.

Table 7: Confusion matrix for case-1.

Events	PCL1	PCL2	PCL3	PCL4	PCL5	PCL6	PCL7	PCL8	PCL9	PCL10	PCL11	PCL12
PCL1	40											
PCL2		40										
PCL3			40									
PCL4				40								
PCL5					39							
PCL6					1	40			1			
PCL7							40					
PCL8								40				
PCL9									39			
PCL10										40		
PCL11											39	
PCL12											1	40
Success rate (%)	100	100	100	100	98.57	100	100	100	98.57	100	98.57	100

Overall success rate: 99.64%.

Classification accuracy is 99%, and specificity is 98.91%; nevertheless, PCL1, PCL2, PCL5, and PCL10 are among the true PQDs that were incorrectly labelled. Performance-wise, the suggested OTQWT-ISVM method outperforms both the WT-ISVM and EWT-ISVM approaches.

The effectiveness of the proposed method has been demonstrated by analyzing the nonstationary power signals of PQDs in real time, despite the presence of noise. All cases include computation time, accuracy percentage, and confusion matrix. The proposed method is reliable, robust, and fast because it yields the same result across cases with varying conditions with higher accuracy and less computational time. There was a greater detection accuracy on PQD data in Case-1. Cases 2–4 with 20 dB, 30 dB, and 50 dB of noise contamination, respectively, have no negative effect on the proposed method's performance. Minimal computational time is fast enough for real-time uses.

4.2.1. Case-1: Process of Classification. In this case, the 1200 extracted datasets are used to evaluate the performance of the proposed approach. Training and test data are used to provide a comprehensive evaluation of performance as shown in Tables 1 and 7.

4.2.2. Case-2: Process of Classification. Here, real-time datasets of PQDs are subjected to a noise addition of 20 dB to test the proposed method for detection and classification accuracy. Numerous studies have found that taking 60% of noisy PQD data for training and 40% for testing is optimal. Tables 8 and 9 show results that support the improved efficiency of the proposed method. Both sets of findings demonstrate the effectiveness of the proposed method, which maintains high precision even in the presence of 20 dB of noise contamination.

4.2.3. Case-3: Process of Classification. PQD datasets with 30 dB of added noise are used to evaluate the effectiveness of the proposed approach based on the OTQWT and ISVM classifiers. Tables 10 and 11 show the obtained results, which demonstrate the effectiveness of the proposed method with a high rate of accuracy and robustness.

Table 8: Classification results of case-2.

Data dimension		Time (in sec.)		Success rate (%)	
Training data	Testing data	Training	Testing	Training	Testing
720	480	0.114	0.0103	99.6	99.52

4.2.4. Case-4: Process of Classification. Here, PQD data with 50 dB of added noise are used to test and defend the proposed method for PQD detection and classification. Tables 2 and 12 summarize the findings. The outcome validates the robustness, reliability, and effectiveness of the proposed approach's classifier under a variety of conditions, reflecting the approach's performance.

4.3. Comparison with Other Methods. The overall accuracy of the proposed method is compared in Table 13 to that of the recently published conventional DWT and ST-based PQD detection techniques. With 50 dB of added noise, OTQWT-ISVM-based classifiers have the highest overall accuracy (99.64%) of all the recently published methods [39]. An accuracy of 94.37 percent, 96.5 percent, and 98.7 percent is achieved, respectively [39], when a DWT feature extraction process is combined with classifiers such as a neural network-based approach, a neuro-fuzzy system, and a rule-based expert system. Zhang et al. [39] proposed a PQD classifier based on WPT and multiclass support vector machine (MSVM) with 96.8% classifying accuracy using only seven types of single PQ disturbances. An enhanced ST with a DT classifier for PQ detection has been proposed [39], with an accuracy of 98.5%. We propose a 97.4% accurate rule-based expert system (RBES) and probabilistic neural network (PNN) using ST-based feature extraction [39]. However, from the perspective of

Table 9: Confusion matrix for case-2.

Events	PCL1	PCL2	PCL3	PCL4	PCL5	PCL6	PCL7	PCL8	PCL9	PCL10	PCL11	PCL12
PCL1	40											
PCL2		40										
PCL3			39									
PCL4				40								
PCL5			1		40			1				
PCL6						39						
PCL7							40					
PCL8								39				
PCL9						1			40		1	
PCL10										40		
PCL11											39	
PCL12												40
Success rate (%)	100	100	98.57	100	100	98.57	100	98.57	100	100	98.57	100

Overall success rate (%): 99.52.

Table 10: Classification results of case-3.

Data dimension		Time (in sec.)		Success rate (%)	
Training data	Testing data	Training	Testing	Training	Testing
720	480	0.115	0.0104	99.65	99.52

Table 11: Confusion matrix for case-3.

Events	PCL1	PCL2	PCL3	PCL4	PCL5	PCL6	PCL7	PCL8	PCL9	PCL10	PCL11	PCL12
PCL1	40											
PCL2		40										
PCL3			39									
PCL4			1	40								
PCL5					38					1		
PCL6					1	40						
PCL7							40					
PCL8					1			40				
PCL9									40			
PCL10										39		
PCL11											40	
PCL12												40
Success rate (%)	100	100	98.57	100	97.14	100	100	100	100	98.57	100	100

Overall success rate (%): 99.52.

Table 12: Classification results of case-4.

Data dimension		Time (in sec.)		Success rate (%)	
Training data	Testing data	Training	Testing	Training	Testing
720	480	0.1157	0.01045	99.6	99.52

real-time applications, the computational burden is the main issue for all the suggested techniques, in addition to the need for higher accuracy and reliable performance. By considering these aspects, the present research has successfully derived computations that exhibit enhanced efficiency resulting in an impressive overall accuracy of 99.64 percent. The proposed method has the additional benefits of being easy to implement and delivering consistent results across a wide range of operational contexts. However, the proposed approach shows less overall accuracy in comparison to ST with FES-CF with a very low gap of deviation of 0.16 percent. This may occur as both methods are tested under many dissimilar conditions like different types and numbers of PQ events and different types of features and noise conditions. However, the proposed approach has the edge over other compared

Table 13: Statistics comparing the accuracy of other common methods.

Methods of classification	Accuracy percentage (50 dB noise addition)
ANN-based DWT	94.37
NFS-based DWT	96.5
MSVM-based WPT	96.8
RBES-based DWT	98.7
DT-based ST	98.5
RBES-based ST	98.2
PNN-based ST	97.4
ST with FES-CF	99.8
Proposed OTQWT with ISVM	99.64

methods in terms of simplicity in formulation, easy way of application, and the possibility to apply for large and complex databases with robustness and reliability in PQ analysis and computation.

5. Conclusion and Future Scope

A novel hybrid approach is proposed to improve the detection and categorization of PQ disturbances. This approach combines OTQWT and ISVM. By applying segmentation and normalization techniques with OTQWT, dominant feature vectors are computed to effectively characterize different types of PQ signals. These feature vectors are then utilized as inputs for classification using an ISVM classifier. To enhance the performance of OTQWT in terms of accuracy and computational efficiency, the integration of PSO is suggested. Furthermore, incremental learning is recommended to improve the effectiveness of the SVM classifier. The proposed hybrid approach has undergone extensive testing on hybrid and individual datasets, considering various noisy conditions ranging from 20 dB to 50 dB. The results demonstrate the efficacy and feasibility of the approach for real-time application.

The key findings of this study are as follows. Firstly, the optimization of TQWT significantly influences the identification of optimal feature sets, resulting in improved accuracy and computational speed. The integration of PSO plays a crucial role in the proposed hybrid method. Secondly, the performance of the ISVM classifier relies on the effective adaptation of continuous training datasets. Incremental learning becomes a critical process for enhancing overall performance. Thirdly, the proposed hybrid method exhibits superior performance. However, in complex distribution systems characterized by power electronics devices, nonlinear loads, noise and harmonic interference in power signals, and monitoring device faults with missing data, the proposed approach may not yield significantly improved results. Moreover, it is crucial to acknowledge that the efficacy of the suggested approach might be influenced by various uncertainties. In such scenarios, alternative methodologies, such as fuzzy logic and deep learning, have the potential to substitute evolutionary-based optimization methods. Looking ahead, the effective management of extensive, intricate, and distorted signals within real-time systems will necessitate the advancement of methodologies. Enhanced techniques will be indispensable for effectively addressing these challenges.

Data Availability

The data used to support the findings of the study can be obtained from the corresponding author upon request.

Conflicts of Interest

The authors declare that they have no conflicts of interest.

References

[1] B. B. Sharma, K. P. Singh, A. Patel, A. Banshwar, N. K. Sharma, and M. Pathak, "Classification of power quality events-an inclusive review," *Journal of Physics: Conference Series*, vol. 1854, no. 1, p. 012020, 2021.

[2] G. S. Chawda, A. G. Shaik, M. Shaik et al., "Comprehensive review on detection and classification of power quality disturbances in utility grid with renewable energy penetration," *IEEE Access*, vol. 8, pp. 146807–146830, 2020.

[3] P. Khetarpal and M. M. Tripathi, "A critical and comprehensive review on power quality disturbance detection and classification," *Sustainable Computing: Informatics and Systems*, vol. 28, 2020.

[4] U. Singh, "A research review on detection and classification of power quality disturbances caused by integration of renewable energy sources," 2020, https://arxiv.org/abs/2009.11426.

[5] M. Mishra, "Power quality disturbance detection and classification using signal processing and soft computing techniques: a comprehensive review," *International Transactions on Electrical Energy Systems*, vol. 29, no. 8, 2019.

[6] "IEEE recommended practice for monitoring electric power quality," *IEEE Std 1159-2019 (Revision of IEEE Std 1159-2009)*, vol. 12, pp. 1–98, 2019.

[7] G. T. Heydt, P. S. Fjeld, C. C. Liu, D. Pierce, L. Tu, and G. Hensley, "Applications of the windowed FFT to electric power quality assessment," *IEEE Transactions on Power Delivery*, vol. 14, no. 4, pp. 1411–1416, 1999.

[8] C. H. Lee and M. S. Tsai, *Application of a Hybrid Method for Power System Frequency Estimation with a 0.2-second Sampled Period*, Preprints, Basel, Switzerland, 2018.

[9] V. Kumar, S. K. Gawre, and T. Kumar, "Power quality analysis using wavelet transform: a review," *International Journal of Innovative Research in Science, Engineering and Technology*, vol. 3, no. 3, pp. 130–136, 2014.

[10] C. Beuter and M. Oleskovicz, "Stransform: from main concepts to some power quality applications," *IET Signal Processing*, vol. 14, no. 3, pp. 115–123, 2020.

[11] M. Liu, Y. Chen, Z. Zhang, and S. Deng, "Classification of power quality disturbance using segmented and modified S-transform and DCNN-MSVM hybrid model," *IEEE Access*, vol. 11, pp. 890–899, 2023.

[12] N. Ramesh Babu and B. Jagan Mohan, "Fault classification in power systems using EMD and SVM," *Ain Shams Engineering Journal*, vol. 8, no. 2, pp. 103–111, 2017.

[13] Y. Xu, Y. Gao, Z. Li, and M. Lu, "Detection and classification of power quality disturbances in distribution networks based on VMD and DFA," *CSEE Journal of Power and Energy Systems*, vol. 6, no. 1, pp. 122–130, 2019.

[14] M. Mishra, R. R. Panigrahi, and P. K. Rout, "A combined mathematical morphology and extreme learning machine techniques based approach to micro-grid protection," *Ain Shams Engineering Journal*, vol. 10, no. 2, pp. 307–318, 2019.

[15] S. Ding, H. Zhao, Y. Zhang, X. Xu, and R. Nie, "Extreme learning machine: algorithm, theory and applications," *Artificial Intelligence Review*, vol. 44, no. 1, pp. 103–115, 2015.

[16] H. Erişti, Ö. Yıldırım, B. Erişti, and Y. Demir, "Automatic recognition system of underlying causes of power quality disturbances based on S-Transform and Extreme Learning Machine," *International Journal of Electrical Power & Energy Systems*, vol. 61, pp. 553–562, 2014.

[17] D. F. Specht, "Probabilistic neural networks," *Neural Networks*, vol. 3, no. 1, pp. 109–118, 1990.

[18] S. Mishra, C. N. Bhende, and B. K. Panigrahi, "Detection and classification of power quality disturbances using S-transform and probabilistic neural network," *IEEE Transactions on Power Delivery*, vol. 23, no. 1, pp. 280–287, 2008.

[19] J. Huang, M. Negnevitsky, and D. Thong Nguyen, "A neural-fuzzy classifier for recognition of power quality disturbances,"

IEEE Transactions on Power Delivery, vol. 2, pp. 609–616, 2002.

[20] M. B. I. Reaz, F. Choong, M. S. Sulaiman, F. Mohd-Yasin, and M. Kamada, "Expert system for power quality disturbance classifier," *IEEE Transactions on Power Delivery*, vol. 22, no. 3, pp. 1979–1988, 2007.

[21] J. G. Decanini, M. S. Tonelli-Neto, F. C. Malange, and C. R. Minussi, "Detection and classification of voltage disturbances using a fuzzy-ARTMAP-wavelet network," *Electric Power Systems Research*, vol. 81, no. 12, pp. 2057–2065, 2011.

[22] M. Biswal and P. K. Dash, "Measurement and classification of simultaneous power signal patterns with an S-transform variant and fuzzy decision tree," *IEEE Transactions on Industrial Informatics*, vol. 9, no. 4, pp. 1819–1827, 2013.

[23] O. P. Mahela and A. G. Shaik, "Power quality recognition in distribution system with solar energy penetration using S-transform and Fuzzy C-means clustering," *Renewable Energy*, vol. 106, pp. 37–51, 2017.

[24] X. Gu and P. P. Angelov, "Self-organising fuzzy logic classifier," *Information Sciences*, vol. 447, pp. 36–51, 2018.

[25] N. Huang, G. Lu, G. Cai et al., "Feature selection of power quality disturbance signals with an entropy-importance-based random forest," *Entropy*, vol. 18, no. 2, p. 44, 2016.

[26] D. De Yong, S. Bhowmik, and F. Magnago, "An effective power quality classifier using wavelet transform and support vector machines," *Expert Systems with Applications*, vol. 42, no. 15-16, pp. 6075–6081, 2015.

[27] B. Eristi, O. Yildirim, H. Eristi, and Y. Demir, "A new embedded power quality event classification system based on the wavelet transform," *International Transactions on Electrical Energy Systems*, vol. 28, no. 9, p. e2597, 2018.

[28] R. Atangana, D. Tchiotsop, G. Kenne, and L. C. Djoufack Nkengfack, "Suitable mother wavelet selection for EEG signals analysis: frequency bands decomposition and discriminative feature selection," *SIPIJ*, vol. 11, no. 1, pp. 33–49, 2020.

[29] M. Sahani, "Detection and classification of power quality events using empirical wavelet transform and error minimised extreme learning machine," *International Journal of Power and Energy Conversion*, vol. 10, no. 4, pp. 452–479, 2019.

[30] I. W. Selesnick, "Wavelet transform with tunable Q-factor," *IEEE Transactions on Signal Processing*, vol. 59, no. 8, pp. 3560–3575, 2011.

[31] K. Thirumala, M. S. Prasad, T. Jain, and A. C. Umarikar, "Tunable-Q wavelet transform and dual multiclass SVM for online automatic detection of power quality disturbances," *IEEE Transactions on Smart Grid*, vol. 9, no. 4, pp. 3018–3028, 2018.

[32] D. Meyer, F. Leisch, and K. Hornik, "The support vector machine under test," *Neurocomputing*, vol. 55, no. 1-2, pp. 169–186, 2003.

[33] W. S. Noble, "What is a support vector machine?" *Nature Biotechnology*, vol. 24, no. 12, pp. 1565–1567, 2006.

[34] R. Kapoor, R. Gupta, L. H. Son, S. Jha, and R. Kumar, "Detection of power quality event using histogram of oriented gradients and support vector machine," *Measurement*, vol. 120, pp. 52–75, 2018.

[35] H. Erişti, Ö. Yıldırım, B. Erişti, and Y. Demir, "Optimal feature selection for classification of the power quality events using wavelet transform and least squares support vector machines," *International Journal of Electrical Power & Energy Systems*, vol. 49, pp. 95–103, 2013.

[36] Z. Liang and Y. Li, "Incremental support vector machine learning in the primal and applications," *Neurocomputing*, vol. 72, no. 10-12, pp. 2249–2258, 2009.

[37] G. Fung and O. L. Mangasarian, "Incremental support vector machine classification," in *Proceedings of the 2002 SIAM International Conference on Data Mining*, pp. 247–260, Philadelphia, PA, USA, April 2002.

[38] M. Sahani, P. K. Dash, and D. Samal, "A real-time power quality events recognition using variational mode decomposition and online-sequential extreme learning machine," *Measurement*, vol. 157, 2020.

[39] H. S. Behera, P. K. Dash, and B. Biswal, "Power quality time series data mining using S-transform and fuzzy expert system," *Applied Soft Computing*, vol. 10, no. 3, pp. 945–955, 2010.